Available online at www.sciencedirect.com
ScienceDirect
European Journal of Mechanics B/Fluids 26 (2007) 258–270

The turbulent flow between two rotating stirrers: similarity laws and transitions for the driving torques fluctuations

Olivier Cadot [a,*], Olivier Le Maître [b]

[a] *Unité de Mécanique de l'Ecole Nationale Supérieure de Techniques Avancées, Chemin de la Hunière, 91761 Palaiseau Cedex, France*
[b] *Laboratoire de Mécanique et d'Energétique, Université d'Evry, 40, rue du Pelvoux, 91020 Evry Cedex, France*

Received 10 October 2005; received in revised form 21 February 2006; accepted 9 May 2006

Available online 30 June 2006

Abstract

Instantaneous torques driving the turbulent flow between two rotating disks equipped with blades and enclosed in a fixed cylindrical cell are measured. The flow is studied by varying the rotational frequency of one stirrer while the other is set to a fixed rotational frequency. Many flow configurations, defined as the rotational frequency ratio S of the disks are studied from the co- to the counter-rotating regimes. For the entire range of S, the driving torques, means and fluctuations give a satisfactory match with similarity laws having no dependence on the Reynolds number. This allows the study to be restricted in the range $S = [-1; +1]$. In the detail, the counter-rotating regime seems to be insensitive to the Reynolds number in the range $-1.33 < S < -0.69$ that correspond to the well known two cell structure configuration. On the contrary, a significant dependence with the Reynolds number is found for the co-rotating regime. Flow transitions marked by strong torque fluctuation crisis are observed for both the co- and counter-rotating regimes. Mean flow visualization elucidates the flow topology corresponding to these transitions.

PACS: 47.27.-i; 05.40.-a

Keywords: Turbulent torque fluctuations; Similarities; Transitions

1. Introduction

The flow between two rotating disks is of practical importance in many industrial devices. From a fundamental point of view, this flow is very complicated, and depends drastically on the boundary conditions [1]. Simple questions such as: does the flow still rotate for very high Reynolds numbers in the counter rotation regime? have stood as a major problem[1] [2]. Most studies, theoretical, experimental or numerical are devoted to the problem initially set by von-Kármán: the flow between two infinite smooth disks. When the disks are not infinite, the condition imposes severe constraints on the flow leading to very different solutions [3]. With smooth disks, it is established that within the case

* Corresponding author.
E-mail address: cadot@ensta.fr (O. Cadot).

[1] This theoretical problem opposed G.K. Batchelor and K. Stewartson in the 50's. Both point of views have been then unified because of the non-unicity of the solutions [3].

0997-7546/$ – see front matter
doi:10.1016/j.euromechflu.2006.05.004

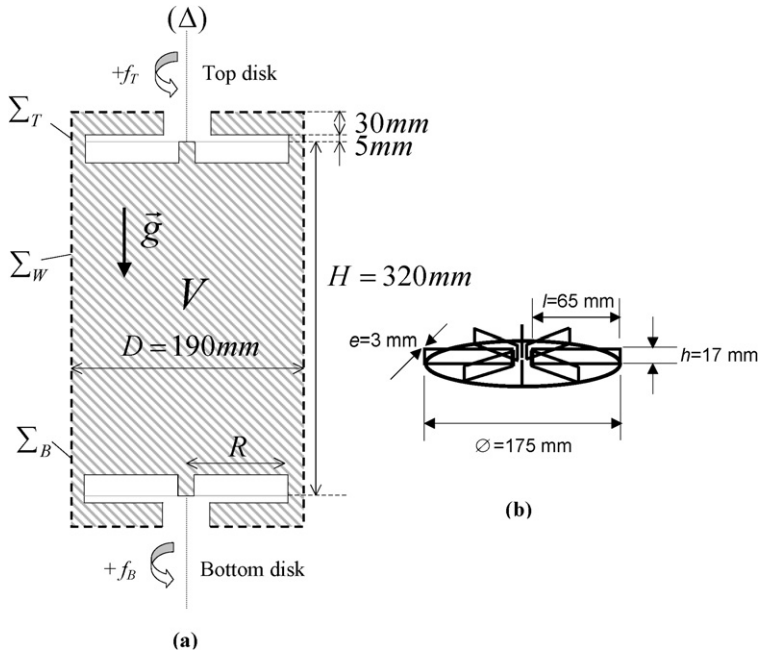

Fig. 1. Cross section (a) of the cylindrical experimental cell. The total volume of fluid is contained within a surface Σ consisting itself of three parts. A fixed part (dashed line) of surface Σ_W corresponding to the wall's cell, and two rotating parts corresponding to Σ_T, the surface of the top disk and Σ_B, the surface of the bottom disk. Detail (b) shows one disk with the arrangement of the six blades.

of the counter-rotating regime, there is a transition for a given Ekman number and rotational frequency ratio from a one cell to two cell structure (primary reported by Lugt and Haussling [4], and checked numerically by Dijkstra and van Heijst [3]). This transition corresponds to the emergence of a detached shear layer on the disk having the slower angular velocity.

The flow considered in this paper, though concerning finite disks, differs from the previous studies because the disks are equipped with blades pushing the flow (see Fig. 1). This type of flow, and especially in the exact counter-rotating regime is now extensively used in the aim of studying fundamental aspects of developed turbulence. The reason comes from appreciable advantages given by a closed flow (compared to classical open flows) and has been successfully used for the comprehension of turbulence in, for instance: dynamical structures observations [5] and characterizations [6], global power fluctuations [7,8], drag reduction by polymer additives [9], passive scalar intermittency [10], particule accelerations [11] and magneto-hydrodynamics turbulence [12]. Particularly, this flow has been found to follow the Kolmogorov K41 scaling (no viscosity dependency) for the global mean power injection (or mean dissipation) [13,14] and the global fluctuation of the injected power for the exact counter-rotating regime ($S = -1$) [8,14].

To our knowledge, only a few articles are devoted to the characterization of the global flow properties in this geometry (disks with blades) for any S. Marié et al. [15] characterized the mean kinetic momentum by means of LDV measurements in the exact counter rotating regime ($S = -1$). Very recently, Ravelet [16,17] explored the flow in the counter-rotating regime ($S \leqslant 0$) by means of mean global torque measurements and PIV velocity measurements and found a global transition from a one cell to a two cells flow for $S = -0.78$ similar to those observed for smooth disks [4].

An interesting issue for fundamentals in turbulence is the properties of the temporal fluctuations of large scale quantities [7]. Our system allows for reliable measurement of torque fluctuations due to turbulence [8,14]. Question as: how does the torque fluctuations depend on the rotational frequency ratio S for both co- and counter-rotating regimes has not been addressed yet.

The aim of the present work is two fold. First, it is a contribution to the characterization of the flow produced between disks with blades having differential rotations (for a wide range of rotational frequency ratio S) which has to be linked with previous available results in the literature about forced flows in the same configuration, but with smooth

disks. Secondly, we seek for relations between the magnitude of the torque fluctuations and the mean flow structure, for a given S, by means of flow visualizations.

The characterization is obtained by mean of instantaneous torque measurement on both disks. We are interested in the evolution of the mean torques and their fluctuations (*rms* value) for both disks versus the rotational frequency ratio S. The present work is organized as follow; the experimental set up is first presented in Section 2 and concerns the experimental geometry, torque measurements and flow visualization. Section 3 is a preliminary and will recall the momentum budget equation for this geometry [15] as well as some symmetry properties of the flow forcing. The results are presented in Section 4 and discussed in three parts in Section 5. These three discussions are about similarity laws, the one to two cells transition for the counter rotating regime and the dependence of the torque fluctuations on the rotational frequency ratio.

2. Experimental set-up

2.1. Experimental cell

Titon and Cadot [14] have previously described this experimental cell in detail. The turbulence is generated in a closed cylindrical cell ($V = 11$ liters) between two rotating stirrers (disk with blades) of radius $R = 8.75$ cm spaced a distance $H = 320$ mm apart (see Fig. 1 for specific sizes). Two DC servomotors regulated by servo amplifiers (from Parvex) independently drive each stirrer. The motors are configured to keep the disks rotating at constant angular velocity Ω, independently of the torque exerted by the turbulence on the disks. This is done by using a tachymetry feedback loop, a regulation system that adapts the torque delivered by the motors to maintain the imposed angular velocity. The time response of the control loop is 0.05 s, implying a high-frequency cut-off of 20 Hz (see [14] for further details). For lower frequencies, the image of the electric current measured as a voltage output of the regulation gives an instantaneous measurement of the torque. The electric current is directly proportional to the torque following the Laplace law. 1 volt of torque signal output corresponds to 0.52 N m. In the following the torques are presented in arbitrary units for which 1 AU of torque $= 0.52$ N m, and the frequencies of rotation are in Hz. The instantaneous torque delivered by each DC servomotor, $\Gamma_{\mathrm{B}}^{\mathrm{M}}(t)$ and $\Gamma_{\mathrm{T}}^{\mathrm{M}}(t)$ are analyzed with a data acquisition board and LABVIEW software.

For the present experiments the working fluid is always water and only the angular velocities on both disks are varied. The Reynolds number reaches at maximum, a magnitude of: $Re = (|\Omega_{\mathrm{B}} - \Omega_{\mathrm{T}}|R^2)/(2\upsilon_{\mathrm{water}}) \leqslant 200\,000$.

2.2. Instantaneous turbulent torque measurements

The drag torque $\Gamma_i(t)$ due to the fluid flow on the disk i ($i = \mathrm{B}$ or T) rotating at the angular velocity Ω_i is computed by subtracting from the motor's torque $\Gamma_i^{\mathrm{M}}(t)$, the torque due to the torques of mechanical friction losses Γ_i^{S} which were measured independently in the empty cell (full of air). We have:

$$\Gamma_i(t) = \Gamma_i^{\mathrm{M}}(t) - \Gamma_i^{\mathrm{S}}(\Omega_i).$$

2.3. Flow visualization

Visualization is realized by seeding the water with particles (PVC powder), having an average diameter of 150 microns and a density $d = 1.35$. Since their density is larger than that of water the particles are also used as indicators of the pressure field in the cell. The cross flow (corresponding to Fig. 1 view) is video taped in a light sheet produced by a 4 Watt Argon laser. The shutter of the camera is set to $1/6$ s and the image rate is $1/50$ s (each frame results from an integration of the flow during a $1/6$ s time duration sliding window). The particles appear white on a black background, and mainly follow the velocity field escaping the large coherent low-pressure region because of their higher density than water.

3. Preliminary

3.1. Preliminary: momentum budget equation

The total flow of volume V is enclosed by a fixed cylinder of surface Σ_W and two rotating disks of surface Σ_B and Σ_T (see Fig. 1). Let $\Sigma = \Sigma_W + \Sigma_B + \Sigma_T$ denote the total surface. The budget equation for the momentum taken from the symmetry axis (Δ) (see Fig. 1) expressed in cylindrical coordinates system reads:

$$\frac{\partial}{\partial t}\iiint_V \vec{r} \wedge \rho\vec{u}\,\mathrm{d}\tau = -\iint_\Sigma (\vec{r} \wedge \rho\vec{u})(\vec{u} - \vec{u}_S)\cdot\vec{n}\,\mathrm{d}S + \iiint_V \vec{r} \wedge \rho\vec{g}\,\mathrm{d}\tau + \iint_\Sigma (\vec{r} \wedge \underline{\underline{\sigma}}\cdot\vec{n})\,\mathrm{d}S, \tag{1}$$

where $\vec{n}$ is the unit vector, normal to the surface and pointing outward the fluid volume, $\vec{u}$ the local velocity of the flow, $\vec{u}_S$ the local velocity of the solid wall, ρ the fluid density, $\vec{g}$ the gravity and $\underline{\underline{\sigma}}$ the total stress tensor. The left-hand side is the rate of change of the total kinetic momentum. The first term on the right-hand side is the flux of kinetic momentum through the total surface and is zero since the surfaces are non-porous implying $\vec{u} - \vec{u}_S = \vec{0}$. The second contribution is the external volume force torque, only due to gravity here, is also zero since this force is uniform and the integration performed with respect to a symmetry axis (Δ) of the system. The third contribution is the momentum of any surface forces applied on the surface total Σ. Since the total surface is basically composed of three individual surfaces (see Fig. 1): this last term involves three contributions:

$$\iint_\Sigma (\vec{r} \wedge \underline{\underline{\sigma}}\cdot\vec{n})\,\mathrm{d}S = \Gamma_B + \Gamma_T + \Gamma_W, \tag{2}$$

Γ_B is the torque exerted on the bottom disk, Γ_T the torque exerted on the top disk and Γ_W is the torque exerted on the inner wall of the fixed cylinder. The budget equation for the kinetic momentum thus becomes:

$$\frac{\partial}{\partial t}\iiint_V \vec{r} \wedge \rho\vec{u}\,\mathrm{d}\tau = \Gamma_B + \Gamma_T + \Gamma_W. \tag{3}$$

By taking the time average of Eq. (3), the left-hand side term becomes zero for stationary turbulence which leads to the simple relationship:

$$\langle\Gamma_B\rangle + \langle\Gamma_T\rangle + \langle\Gamma_W\rangle = 0. \tag{4}$$

The top and bottom time-averaged torques are strongly correlated by the torque exerted on the inner wall of the cylinder.

3.2. Symmetries

There are two symmetries of interest in this study. The first is in respect of the rotational direction (that we will refer as the *rotational direction symmetry*) and the second to the top and bottom exchange (that we will refer as the *inversion symmetry*).

The rotational direction symmetry is expressed as:

$$\begin{aligned}\Gamma_B(f_B = f_0;\, f_T = f) &= -\Gamma_B(f_B = -f_0;\, f_T = -f),\\ \Gamma_T(f_B = f_0;\, f_T = f) &= -\Gamma_T(f_B = -f_0;\, f_T = -f)\end{aligned} \tag{5}$$

and the inversion symmetry is expressed as:

$$\Gamma_B(f_B = f_0;\, f_T = f) = \Gamma_T(f_B = f;\, f_T = f_0). \tag{6}$$

4. Results

4.1. Turbulent torques exerted on the disks vs. the rotational frequency ratio

A typical experiment consists of a series of measurements that we call a run (see Table 1). For a run, we set the rotational frequency of one of the disks to f_0 and vary the other one with a rotational frequency f. When a stationary

Table 1
The three experimental runs #1, #2 and #3 with the corresponding ranges of the rotation frequencies for both top and bottom disks. The parameter S is the frequency ratio

	f_B	f_T	$S = f/f_0$	$S' = 1/S$
Run #1	$f_0 = 5.8$ Hz	-10.6 Hz $< f <$ 11.5 Hz	$[-1.83; 1.98]$	$[\ldots; -0.54] \cup [0.50; \ldots]$
Run #2	-10.8 Hz $< f <$ 10.6 Hz	$f_0 = 5.8$ Hz	$[-1.86; 1.83]$	$[\ldots; -0.54] \cup [0.55; \ldots]$
Run #3	$f_0 = 4.5$ Hz	-10.2 Hz $< f <$ 10.9 Hz	$[-2.26; 2.41]$	$[\ldots; -0.44] \cup [0.41; \ldots]$

regime is reached, we measure the time averaged torque of the bottom disk $\langle \Gamma_B \rangle$, and the top disk $\langle \Gamma_T \rangle$. The typical fluctuations of the torques are measured as the root mean square torques of both forcing devices, we denote them by $\delta\Gamma_T$ for the top disk and $\delta\Gamma_B$ for the bottom disk:

$$\delta\Gamma_T = \sqrt{\langle \Gamma_T^2 \rangle - \langle \Gamma_T \rangle^2} \quad \text{and} \quad \delta\Gamma_B = \sqrt{\langle \Gamma_B^2 \rangle - \langle \Gamma_B \rangle^2}.$$

The time durations on which the averagings are performed are long enough (typically 1 to 2 minutes depending on the rotation frequencies) to insure a good statistical convergence of the torque fluctuations. The measurements are repeated for different values (about 110 values) of f in the range $-2f_0$ and $+2f_0$. Three experimental runs were performed (see Table 1); run #1 and run #2 have an identical fixed rotational frequency f_0, but it is imposed by the bottom disk in run #1 while it is imposed by the top disk in run #2. In run #3, as in run #1, the fixed rotational frequency is imposed by the bottom disk but with a smaller magnitude. The results are displayed versus the rotational frequency ratios either defined as: $S = f/f_0$ or $1/S = f_0/f$, where f_0 always refers to the fixed frequency and f to the variable frequency of the run. Table 1 lists the variations of both quantities for the three experimental runs.

The rotational frequency ratio S characterizes the flow configuration (for instance: $S = +1$ for exact co-rotation). If both the top and bottom rotational frequencies are multiplied by the same factor, S remains unchanged but the Reynolds number is different. Then, two measurements at equal S in run #1 and run #3, which have different f_0 imposed at the same motor, allow for a direct comparison of the torque characteristics at identical flow configuration but different Re. Moreover, in a given run one frequency is held fixed while the other is varied (see Table 1). As a consequence, each run usually investigates a flow configuration twice due to the inversion symmetry of the experiment. For instance, in run #3, measurements made at $S = -2$($f_B = 4.5$ Hz; $f_T = -9$ Hz) and for $S = -1/2$($f_B = 4.5$ Hz; $f_T = -2.25$ Hz) correspond to the same flow configuration but different Re. Thus, there are two ways to vary the Reynolds number at fixed flow configuration: by selecting a different f_0 (as done in run #1 and #3) or by exchanging S by $1/S$ in the same run. Finally, run #1 and run #2 having the same f_0, but imposed to opposite motors, a measurement for one disk at a flow configuration S (resp. $1/S$) in run #1 should be exactly equal to the measurement for the opposite disk at $1/S$ (resp. S) in run #2, because their Reynolds numbers are equal and because of the symmetry relation (6). This last correspondence allows for a verification of the actual symmetry properties of the experimental system.

In Figs. 2(a) and 2(b), we reported respectively the mean and the fluctuating torques of the top and bottom forcing devices as a function of $S = f/f_0$. Torques are divided by the square of the fixed rotational frequency f_0, to define a "dimensionless torque" with respect to the only variable quantities of the experiments, say the frequencies of rotation. The dimensionless torque is similar to a friction coefficient. However it could be useful for comparison with other works to introduce the dimensionless κ torque defined as $\Gamma = \kappa\rho\Omega_0^2 R^5$. The conversion from our arbitrary "dimensionless torque" presented in our Figs. 2–4 and κ is: $\kappa = 2.81 \times 1$ AU of Γ/f^2.

The symmetry properties of the apparatus is first checked in Fig. 2(a) for the mean torque, by comparing $\langle \Gamma_B \rangle / f_B^2$ [resp. $\langle \Gamma_T \rangle / f_B^2$] measured in run #1 at S to $\langle \Gamma_T \rangle / f_T^2$ [resp. $\langle \Gamma_B \rangle / f_T^2$] measured in run #2 at $1/S$, as discussed above. To ease the comparison, the measurement of run #2 are plotted as a function of $S' = 1/S$, such that the symmetry is directly deduced from the fact that the solid lines (measurements of run #1) and the crosses (measurements of run #2) are superimposed.

Also, the measurements of run #3 (circles) and run #2 (lines), both plotted as functions of S, while being performed at different reference frequencies f_0 clearly superimpose too, suggesting that the "non-dimensional" torques as defined above only depend on the rotational frequency ratio S and not on the Reynolds number.

The torque fluctuations are shown in Fig. 2(b); even if the superimposition of the measurements of run #1 (lines) and those of run #2 (plotted as a function of $S' = 1/S$ with crosses) is not as good as for the mean torque in Fig. 2(a),

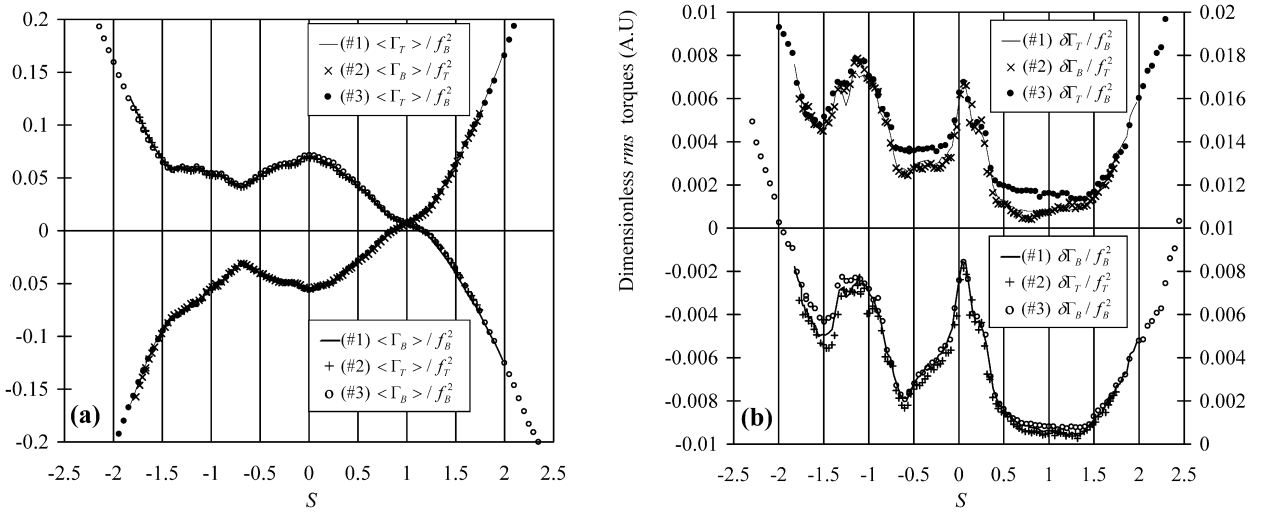

Fig. 2. Torque measurements versus the rotation frequency ratio S. The dimensionless time averaged torques (a) $\langle \Gamma_T \rangle / f_B^2$ and $\langle \Gamma_B \rangle / f_B^2$ are displayed for two different fixed rotational frequencies of the bottom disk (run #1 and run #3, see Table 1). In (a), $\langle \Gamma_B \rangle / f_T^2$ and $\langle \Gamma_T \rangle / f_T^2$ measured in run #2 are respectively the symmetric (see Eq. (6)) of $\langle \Gamma_T \rangle / f_B^2$ and $\langle \Gamma_B \rangle / f_B^2$ measured in run #1. The dimensionless torque fluctuations (b), $\delta\Gamma_T / f_B^2$ and $\delta\Gamma_B / f_B^2$ are displayed for two different fixed rotational frequencies of the bottom disk (run #1 and run #3, see Table 1). In (b), $\delta\Gamma_B / f_T^2$ and $\delta\Gamma_T / f_T^2$ measured in run #2 are respectively the symmetric (see Eq. (6)) of $\delta\Gamma_T / f_B^2$ and $\delta\Gamma_B / f_B^2$ measured in run #1.

the inversion symmetry is checked rather satisfactorily. It can be concluded that the experimental set-up provides quite accurate measurements of the instantaneous torques for run #1 and run #2. However, there is much significant discrepancy in the measured fluctuations of the top disk torque between run #3 (filled circles) and run #2. We believe that this discrepancy is due to small axisymmetry defects in the mechanical apparatus inducing spurious (non-hydrodynamical) fluctuations which become significant when the hydrodynamic torque has low magnitude. The contribution of these defects to the measured fluctuations is essentially negligible in run #1 and run #2. In run #3 on the contrary, experiments are performed at a frequency f_0 lower than for run #1 and run #2, with lower hydrodynamical torques and noticeable impact of the defects on the measurements as a result, especially in the low fluctuations magnitudes around $S = -1/2$ and $S = 1$. In fact, the top motor is probably plagued by an axisymmetric mis-balance causing an overestimation of the torque fluctuations at low rotational frequencies. This claim is supported by the fact that these defects have no impact on the mean torque measurements and the much better agreement between run #1 and run #3 for the measured fluctuations on the bottom disk.

Except this minor defect in run #3, the measured torque fluctuations when non-dimensionalized by the square of the rotational frequency clearly exhibit a dependence on the rotational frequency ratio S only. This observation can be further verified from the data of a single run (run #1 for instance). As explained above, in a run a flow configuration is generally inspected twice (at S and $1/S$) corresponding to two different Reynolds numbers (the largest being for S if $|1/S| < 1$ and vice versa). Then if the torque characteristics are actually *Re* independent, equivalent flow configurations should lead to consistent measurements for S and $1/S$. To check the inversion consistency, one has to compare properly renormalized torques characteristics measured on opposite disks. The results of such consistency analysis is presented in Fig. 3 for the measurements of run #1. To make easier the appreciation of the consistency, all the data are plotted in the range $-1 \leqslant S \leqslant 1$. The measurements that were actually performed for $-1 \leqslant S \leqslant 1$ are directly plotted using lines, while those corresponding to an actual experiment with $|S| \geqslant 1$ are first transformed to their symmetric counterpart before being plotted using crosses. Thus, the consistency can be directly appreciated from the agreement between the lines and the crosses. Fig. 3(a) confirms the expected consistency of the mean torque measurements for run #1 and so support the weak dependence of the mean driving torque with regard to the Reynolds number. A similar conclusion can be drawn from the inspection of the torque fluctuations reported Fig. 3(b). However, a better superimposition is found in the counter-rotating regime compared to the co-rotating regime. This effect could be ascribed to the viscosity as discussed below.

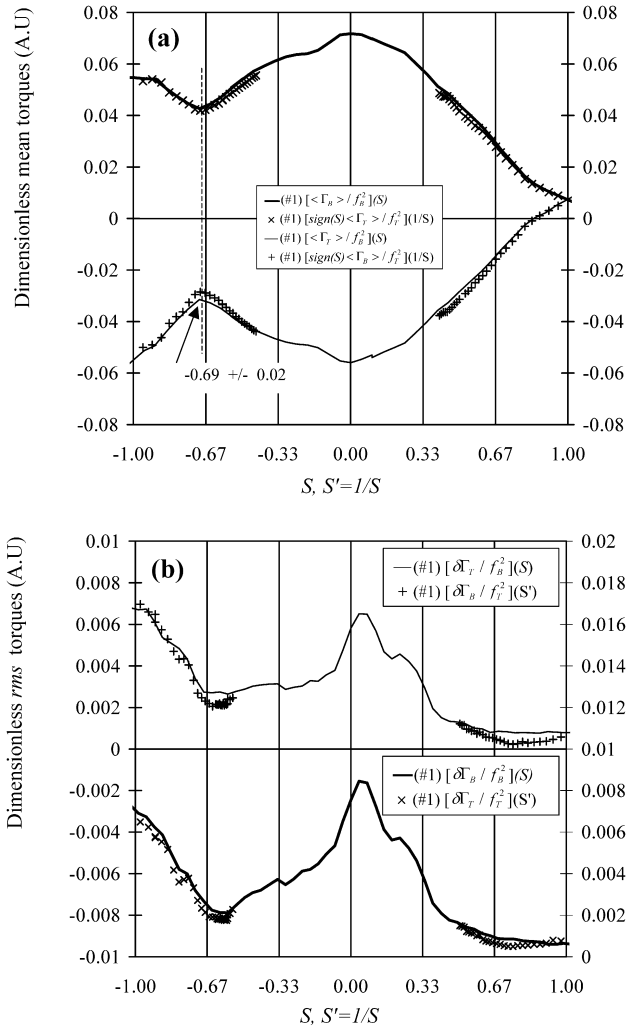

Fig. 3. Similarity laws checking for the dimensionless averaged torques (a) and the dimensionless fluctuation torques (b) for run #1 versus $S \in [-1, 1]$. The measurements indicated by crosses are deduced from the torque measurements for $S \leqslant -1$ and $S \geqslant 1$ and are plotted vs. $S' = 1/S$. For this representation the two symmetries of Eqs. (5) and (6) are needed (see text).

4.2. Torque exerted on the inner cell wall

The time averaged torque exerted on the inner wall of the cylindrical cell is computed from Eq. (4). We first consider the continuous lines in Fig. 4 that show the non-dimensional wall torque $\langle \Gamma_W \rangle / f_B^2$ for both run #1 and #3 versus S. The modulus of the non-dimensional torque plays the same role as a friction coefficient. On Fig. 4, we can see that both non-dimensional wall torques deviate significantly from each other showing a clear Reynolds number dependence. Run #3 (performed at a lower Reynolds number) always has a larger non-dimensional torque modulus than run #1 (performed at a larger Reynolds number at a given S). The larger the Reynolds number, the smaller the modulus of the non-dimensional torque or the friction coefficient. This dependence with Re is consistent with the friction law measured in flat plate at zero incidence. Now if we look closer in the case of the counter-rotating regime, we find both runs to have a better superimposition in a range around $S = -1$, indicating a small dependence on Re. We can also check the dependence on Re by changing S by $1/S$ for a given run (this is done by applying the symmetries of Eqs. (5) and (6) on both runs as in Fig. 3). We obtained the crosses for run #1 and the straight crosses for run #3. We also observed that crosses and lines all collapse in a range around $S = -1$. The flow configuration corresponding to $S = -1$ is particular. The wall torque here is zero since it results from the two opposite frictions due

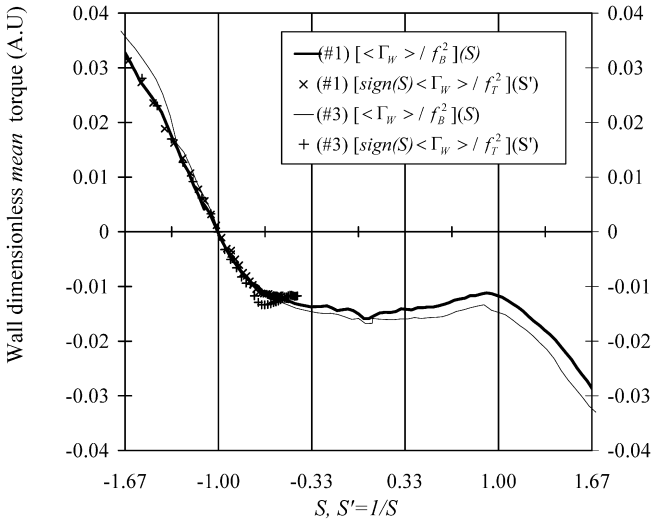

Fig. 4. Dimensionless averaged torque over the inner smooth wall versus $S \in [-1, 1]$ for run #1 and #3. The measurements indicated by crosses are deduced from the measurements within the ranges $S \leqslant -1$ and $S \geqslant 1$ and are plotted vs. $S' = 1/S$. For this representation the two symmetries of Eqs. (5) and (6) are needed (see text).

to the opposite rotations. For this case, it is impossible to state on the dependency of the friction with *Re*. For the other flow configurations, of the range $-1.33 < S < -0.67$, the wall torque does not seem to depend on *Re*.

4.3. Visualization of the flow as a function of S

We have so far quantified the torque's magnitudes, symmetries and scaling, we now turn to the complex structure of the torques evolution with the frequency ratio. Our idea is to understand the torque behavior with the help of the global time averaged flow visualization. We restrict the study between $-1 < S < +1$ only (this restriction is justified because of the symmetries and the scaling laws properties displayed in Fig. 3). In Figs. 5 and 6 the frequency of the bottom disk is set to 4.5 Hz.

We first focus on the counter-rotating regime. Fig. 5 shows the flow section for 3 negative values of S and for $S = 0$. The first picture in Fig. 5 shows the exact counter-rotating regime $S = -1$. The time averaged flow consists of a cell point centered in the middle of the cell. Above and below this stagnation point we can observe four cell structures that are actually the cross section of two re-circulation tores. In the literature [1–5] on rotating disks, this flow topology is referred as a two cells flow structure. They are the result of the radial ejection with a central suction on both disks. The separation of both tores is marked by a strong radial jet coming from the cylinder wall to the centre. For $S = -1$ the separation is exactly in the middle plan of the cylinder. On the next picture, $S = -0.53$, the separation moves above (actually, closer to the lowest velocity rotating disk) and only one re-circulation tore is now observable near the bottom disk. The flow at $S = -0.2$ is very similar to that of $S = -0.53$. At $S = 0$, we observe a strong coherent jet orientated from the top disk to the bottom disk. A very surprising feature is the presence of a very strong depression (appearing black) at the centre of the top disk (that is not rotating).

For the co-rotating regime, the flow also seems to encompass transitions. At $S = 0.2$, the strong depression on the top disk disappears, and reappears again for $S = 0.35$. In this case, the vertical jet becomes much weaker. For larger values of S, the vertical jet is even not observable anymore. From $S = 0.65$ to $S = 1$ we observe the increase of a large depression along the vertical symmetry axis of the cylinder. For the values of $S < 1$, the depression is concentrated only around the cylinder axe, while it takes the entire volume of the cylinder at $S = +1$. At $S = +1$, all the particles are localized in the mid plan and near the wall, where the flow rotation is the weakest (due to the dissipation occurring at the cylinder wall). The small white regions appearing in the middle are air bubbles introduced in the flow through a leak in the watertight joints.

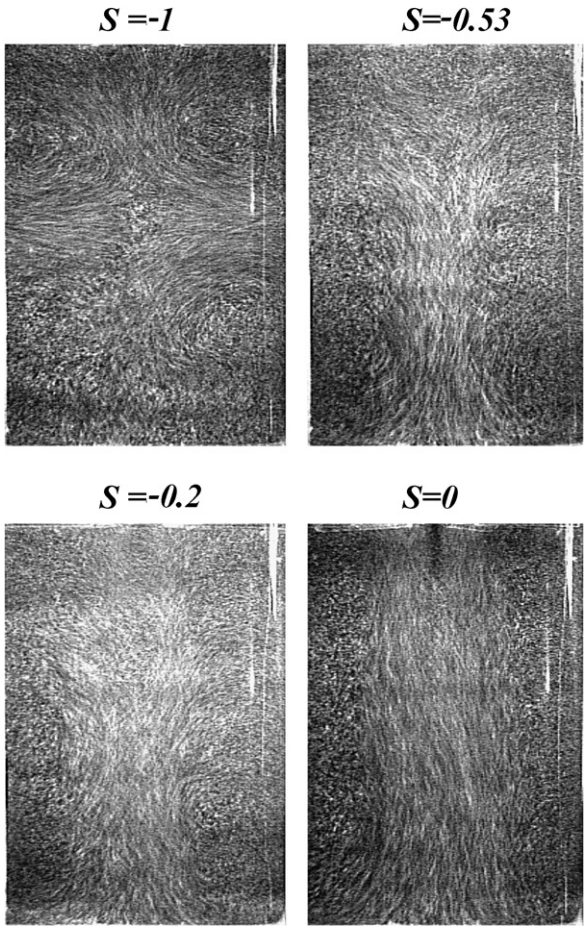

Fig. 5. Flow visualization of the counter-rotating regime, $S \leqslant 0$. The bottom disk's rotational frequency is set to 4.5 Hz.

5. Discussion

5.1. Similarity laws for mean and fluctuating torques

The mean torques on both disks are found to depends mostly on the rotational frequencies (Figs. 2(a), 3(a)). We can thus model the mean torques as:

$$\Gamma_{\mathrm{B}}(f_{\mathrm{B}}; f_{\mathrm{T}}) = f_{\mathrm{B}} f_{\mathrm{T}} H_{\mathrm{T}}(S) \quad \text{and} \quad \Gamma_{\mathrm{T}}(f_{\mathrm{B}}; f_{\mathrm{T}}) = f_{\mathrm{B}} f_{\mathrm{T}} H_{\mathrm{B}}(S),$$

where $H_{\mathrm{T}}(S) = H_{\mathrm{B}}(1/S)$ (due to the inversion symmetry) is a non-dimensional function which depends only on the geometry of the system. At first order, this system does not depend on the viscosity (in the range of our measurements) whatever the frequency ratio. This observation was already reported [13] but only for $S = -1$ who ascribed this effect to an inertial stirring of the turbulence. The system actually seems to be inertial even for a larger range of frequency ratios. However, if we look closer, some significant effect due to the viscosity (i.e. *Re*) is found on the total torque exerted on the inner wall of the cylinder (Fig. 4). In this case, a large amount of the total energy is dissipated on the smooth wall. For instance for $S = 1$, the bulk rotates as a solid body and most of the strain, hence the dissipation is only localized on the inner smooth wall. The friction law is here similar to what is reported in smooth plates, where it is a function of Reynolds number; the larger the Reynolds number, the smaller the friction coefficient [18]. In addition, it is interesting to note that for the counter-rotating regime around $S = -1$ (approximately $-1.33 < S < -0.67$), there is a domain in which the total wall torque coefficient does not depend on the Reynolds number (Fig. 4). This result seems in contradiction with the friction law of smooth plates at zero incidence [18]. The friction law being essentially related to the thickness of the turbulent boundary layer, which decreases as the Reynolds number increases, it leads us

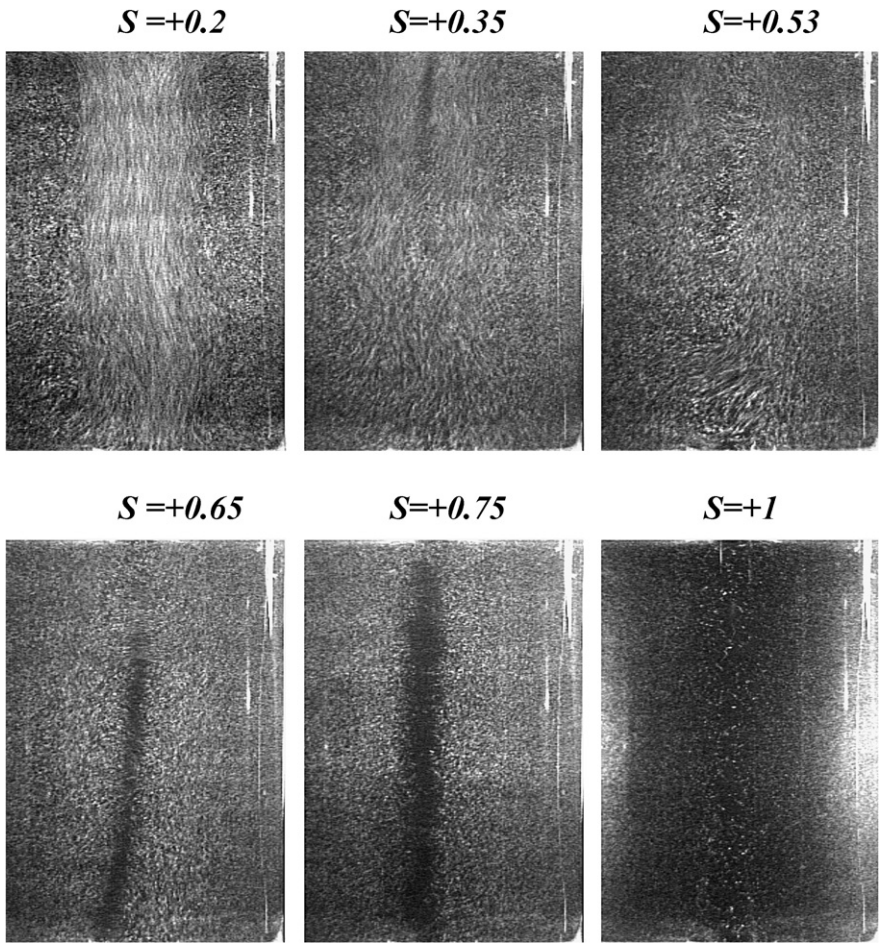

Fig. 6. Flow visualization of the co-rotating regime $S > 0$. The bottom disk's rotation frequency is set to 4.5 Hz.

to assume that the constant friction reported in our measurements could be due to a Reynolds-independent thickness of the turbulent boundary layer over the inner wall of the cylinder. This effect would be due to the strong elongational stress at the wall between the cells as suggested by Fig. 5 at $S = -1$. Further investigations are yet to be performed to confirm or to find another explanation for this effect.

We also measured the fluctuations of the driving torque for any flow configurations from the co- to the counter-rotating regime. From Figs. 2(b) and 3(b), we can deduce that the fluctuations do not depend on the Reynolds number in the counter-rotating regime ($S < 0$). Since the averaged torques are also *Re* independent, the rate of fluctuations is then a constant that only depends on S. These observation is consistent with previous results that were obtained for $S = -1$ only [14]. For the co-rotating regime, we think that there is a dependence with the Reynolds number. Since in Fig. 3(b), crosses are performed at larger Reynolds number, the experiment indicates that the fluctuations decrease as *Re* increases.

5.2. *The transition at* $S = -0.69$

One of the most striking transition that can be observable on the torque measurements occurs at $S = -0.69$ (or $S = -1.45$) in Figs. 2 and 3. This transition can be related in the flow to the transition from a one cell flow structure to a two cell flow structure. Such transition has already been reported in cases of counter-rotating smooth disks [3,4]. A two cell structure corresponds to a situation where the centre part of both disks sucks the flow. The two cells are clearly observable in Fig. 5(a) for $S = -1$ and correspond to the sections of two re-circulation tores. A one cell structure corresponds to a situation where the centre part of the disk having the larger frequency rotation sucks the

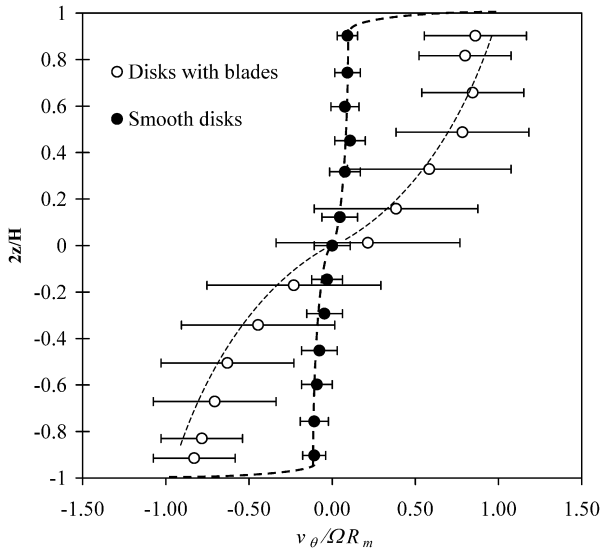

Fig. 7. Laser Doppler velocimetry measurements of the orthoradial velocity profile $v_\theta(2z/H)$ along a vertical axis located at $R_m = 0.7R$. $z = 0$ defines the middle plan of the cylindrical cell and H is the distance separating both disks. The vertical bars correspond to the *rms* values of the velocity. When the disks are equipped with blades, the velocity profile corresponds very schematically to the dashed thin line, that joins the boundary condition at the disks without any velocity gradient. In contrast, with smooth disks, the velocity profile should join the boundary condition at the disks through a thin viscous boundary layer as depicted by the dashed thick line.

flow, while the centre part of the other disk having a lower rotation frequency ejects the flow. Such a situation is observable in Fig. 5(d) for $S = 0$ where only one recirculation torus is present. In previous works concerning smooth disks, the transition is found to depend strongly on the Ekman number but to be independent of the aspect ratio of the experiment [3,4]. The Ekman number compares the thickness of the boundary layer on the disk to the distance between both disks. It is defined as: $Ek = (\delta/H)^2$. In smooth disks experiment the velocity gradient are located in the boundary layer (see Fig. 7) on the disk and decreases (as the Ekman number) when the Reynolds number increases. For an inertially driven flow (disks with blades), the situation is very different since the mean flow does not present any velocity gradients in the vicinity of the disks but are distributed in the bulk (see Fig. 7). There is in this case an effective [19] boundary layer in the bulk that does not depend on the Reynolds number which should correspond to a very large Ekman number. Dijkstra and van Heijst [3] computed analytically the critical value for the transition S_c in the case $Ek \to +\infty$ and found $S_c = -2/3$. The value is very close to ours (-0.69 compared to -0.67), it then confirms the similitude between the smooth disks flow with a large viscosity (large Ek) and the mean flow of the inertially driven turbulent flow. The reason for this similarity is the large efficiency in both cases of the momentum transport in the flow. We can notice that the critical value obtained in our experiment is slightly larger. This effect could be related to the detail of the azimuthal velocity profile that is linear in the flow produced by smooth disks at infinite Ekman number and having a tangent hyperbolic shape in our flow (see Fig. 7). The experiment of Ravelet [16] confirms the role of the mean flow detail since a transition at $S = -0.78$ is found with their geometry.

5.3. The torque fluctuations versus S

In Fig. 3(b), the torque fluctuations present drastic changes versus the rotational frequency ratio S. There are two very distinct maxima at $S = -1$ and $S = 0.06$. A third local maximum is also observable at $S = 0.23$. For the exact counter rotating regime, $S = -1$; the mean flow corresponds to a stagnation point in the middle of the cell (see Fig. 5(a)). This type of flow is known to be very unstable [20] which then could explain the large magnitude of the fluctuations. For larger rotational frequency ratio, the torque fluctuations have a minima for $S = -0.60$ which is close to the transition between the one and the two cells flow structures (see discussion 5.2). The torque fluctuations then increase continuously from $S = -0.6$ to $S = +0.06$ where the magnitudes of the fluctuations are comparable to those at $S = -1$. The flow instationarity here is probably related to the vortex breakdown dynamics that appear in the rotor stator configuration [21].

For larger values of S, the fluctuations decreases mostly until the co-rotating regime $S = +1$. However, a transition is observable around $S = 0.2$. This transition could be related to the appearance of a second recirculation cell similarly to the counter-rotating regime (read discussion 5.2). Actually it is known [22] that if the cylinder is fixed, both disks should produce a suction leading to a two cell flow structure for $S = +1$. The flow should then undergo a transition between $S = 0$ and $S = +1$. On our visualization, it is difficult to check this idea. The picture $S = 0.2$ in Fig. 6 gives some indications. One can observe a strong suction due to the top disk that rotates the fastest, but also a small torus section on the bottom disk, showing that the bottom disk sucks the flow as well. This figure then suggests that the flow consist in a two cells structure at $S = 0.2$.

6. Conclusion

The measurements of the torques driving the turbulent flow for this geometry provide results about the similarity laws. The flow is found to be fully inertial for any contribution of the torques (disks and smooth inner cylinder wall) for the rotation angular velocity ratio in the range $-1.33 < S < -0.67$. This range corresponds to the existence of two cells in the bulk. We then believe the strong elongational stress at the wall to be responsible for this inertial behavior. For this range the similarity laws for the torques are then simple; whatever the Reynolds number explored, the dimensionless torque (mean and fluctuation) only depend on S. For a given ratio S, the dimensionless torques of the bottom and the top stirrer respectively are identically equal to those obtain for the ratio $1/S$ of the top and the bottom stirrer respectively. For rotational frequency ratios outside this range, we find the energy injection to depend on the viscosity, mainly due the torque exerted on the inner smooth wall that behave now as a conventional turbulent friction law. However, the similarity laws discussed above are reasonably followed and a good representation of torques can be given in the range $S = [-1; +1]$. Global transitions are observed versus S, shown by abrupt changes in both the mean torques and the torques fluctuations. A transition occurring at $S = -0.69$ is clearly identified corresponding to the well known one to two cell transition. A similar transition is also detected in the co-rotating regime ($S > 0$).

Acknowledgements

We are grateful to Arnaud Chiffaudel for his critical reading of the manuscript. The authors are grateful to J.R. Wrightson.

References

[1] P.J. Zandbergen, D. Dijkstra, Von Karman swirling flows, Annu. Rev. Fluid Mech. 19 (1987) 465.
[2] G.K. Batchelor, Note on a class of solutions of the Navier–Stokes equations representing steady rotationally-symmetric flow, Quart. J. Mech. Appl. Math. 4 (1951) 29;
K. Stewartson, On the flow between two rotating coaxial disks, Proc. Cambridge Philos. Soc. 42 (1953) 333.
[3] D. Dijkstra, G.J.F. van Heijst, The flow between two finite rotating disks enclosed by a cylinder, J. Fluid Mech. 128 (1983) 123.
[4] H.J. Lugt, H.J. Haussling, Development of flow circulation in a rotating tank, Acta Mech. 18 (1973) 255.
[5] S. Douady, Y. Couder, M.-E. Brachet, Direct observation of the intermittency of intense vorticity filaments in turbulence, Phys. Rev. Lett. 67 (1991) 983.
[6] O. Cadot, S. Douady, Y. Couder, Characterization of the low pressure filaments in a three-dimensional shear flow, Phys. Fluids 7 (3) (1995) 630.
[7] R. Labbé, J.-F. Pinton, S. Fauve, Power fluctuations in turbulent swirling flows, J. Phys. II (France) 6 (1996) 1099.
[8] O. Cadot, J.H. Titon, On the relationship of the injected power between constant torque forcing constant velocity forcing of fully turbulent flow, Phys. Fluids 16 (6) (2004) 2140.
[9] O. Cadot, D. Bonn, S. Douady, Turbulent drag reduction in a closed flow system: boundary layer vs. bulk effects, Phys. Fluids 10 (2) (1998) 426.
[10] F. Moisy, H. Willaime, J. Andersen, P. Tabeling, Passive scalar intermittency in low temperature helium flows, Phys. Rev. Lett. 86 (21) (2001) 4827.
[11] G.A. Voth, A. La Porta, A.M. Crawford, J. Alexander, E. Bodenschatz, Measurement of particle accelerations in fully developed turbulence, J. Fluid Mech. 469 (2002) 121.
[12] F. Pétrélis, M. Bourgoin, L. Marié, A. Chiffaudel, S. Fauve, F. Daviaud, P. Odier, J.-F. Pinton, Non linear induction in a swirling flow of liquid sodium, Phys. Rev. Lett. 90 (17) (2003) 174501.
[13] O. Cadot, Y. Couder, A. Daerr, S. Douady, A. Tsinober, Energy injection in closed turbulent flow: stirring through boundary-layers versus inertial stirring, Phys. Rev. E 56 (1997) 427.

[14] J.H. Titon, O. Cadot, The statistics of power injected in a closed turbulent flow: constant torque forcing vs. constant velocity forcing, Phys. Fluids 15 (3) (2003) 625.
[15] L. Marié, F. Daviaud, Experimental measurement of the scale-by-scale momentum transport budget in a turbulent shear flow, Phys. Fluids 16 (2) (2004) 457.
[16] F. Ravelet, Bifurcation globales hydrodynamiques et magnétohydrodynamiques dans écoulement de von Karman turbulent, PhD thesis of Ecole Doctorale de l'Ecole Polytechnique, 2005.
[17] F. Ravelet, L. Marié, A. Chiffaudel, F. Daviaud, Multistability and memory effect in a highly turbulent flow: experimental evidence for a global bifurcation, Phys. Rev. Lett. 93 (2004) 164501.
[18] H. Schlichting, K. Gersten, Boundary Layer Theory, Springer, 2000.
[19] O. Cadot, D. Bonn, S. Douady, Turbulent drag reduction in a closed flow system: boundary layer vs. Bulk effects, Phys. Fluids 10 (2) (1998) 426.
[20] B. Andreotti, S. Douady, Y. Couder, An experiment on two aspects of the interaction between strain and vorticity, J. Fluid Mech. 444 (2001) 151.
[21] A. Spohn, M. Mory, E.J. Hopfinger, Experiments on vortex breakdown in a confined flow generated by a rotating disc, J. Fluid Mech. 370 (1998) 73.
[22] J.A.C. Humphrey, D. Gor, Experimental observations of an unsteady detached shear layer in enclosed corotating flow, Phys. Fluids A 5 (10) (1993) 2438.